Redshift of surface plasmon modes of small gold rods due to their atomic roughness and end-cap geometry

Carlos Pecharromán,[1] Jorge Pérez-Juste,[2] Gustavo Mata-Osoro,[1] Luis M. Liz-Marzán,[2] and Paul Mulvaney[3]
[1]*Instituto de Ciencia de Materiales de Madrid, CSIC, Cantoblanco, Madrid 28049, Spain*
[2]*Departamento de Química Física and Unidad Asociada CSIC, Universidade de Vigo, 36310 Vigo, Spain*
[3]*Chemistry School, University of Melbourne, Parkville, Victoria 3010, Australia*
(Received 27 June 2007; revised manuscript received 2 October 2007; published 17 January 2008)

We use the surface integral technique for calculation of the extinction spectra of small metal particles of different shapes. We consider in detail different nonellipsoidal geometries in the electrostatic limit, including cylinders and a variety of capped cylinders. It is shown that different capping geometries have pronounced effects on the energy and intensity of the longitudinal surface plasmon mode. In addition, we propose that atomic scale surface roughness may also be an important determinant of the surface plasmon peak energy. A surface roughness of 0.10, equivalent to around two atomic layers, can generate redshifts in surface plasmon modes similar in magnitude to the redshifts induced by changes in the end-cap geometry.

DOI: 10.1103/PhysRevB.77.035418 PACS number(s): 78.67.Bf, 41.20.Cv, 73.20.Mf, 78.68.+m

I. INTRODUCTION

Over the last ten years, a number of chemical methods have been developed for the chemical synthesis of small metal rods,[1–11] nanoscale triangular prisms,[12] pentagons, and even cubes.[13] This growing sophistication in metal nanocrystal synthesis is opening up numerous opportunities to design "plasmonic" structures in which the conduction electron resonances are manipulated through changes in particle size, shape, and morphology. Comparatively small changes in particle morphology can shift such surface plasmon resonances from the UV into the NIR region, so that the perceived color of such materials can be controlled by fabrication of nanomaterials of different shapes. Of particular interest at present are gold rods, which can be grown in solution with a wide range of aspect ratios. It has been common to treat these particles as ellipsoids, which enables their optical properties to be calculated analytically. However, electron microscopy reveals these rods to be more or less cylindrical, and it is questionable whether the ellipsoid model is accurate. However, while there is growing recognition that rodlike particles are not well modeled as ellipsoids, it is also not clear that they should necessarily be better modeled as flat cylinders. High-resolution microscopy reveals a range of end-cap geometries as we discuss.

Several groups have recently employed computational methods to calculate the optical properties of gold cylinders including the T matrix,[14] finite difference time domain, boundary element,[15] and discrete dipole approximation (DDA) methods.[16–21] Such methods are quite CPU intensive, and the calculation efficiency depends on the system contrast, i.e., the ratio of the dielectric function of the matrix to that of the particle.[22] In fact, several groups[18,23] have exploited the use of DDA calculations to understand the effects of particle shape and the dielectric environment on the surface plasmon longitudinal (SPL) peak position, but none of them has achieved a real match between experimental SPL wavelengths and the calculated peak positions based on the real shape of the nanorods as determined by transmission electron microscopy (TEM). In general, the experimentally observed peak positions are always at longer wavelengths than predicted by theory. Prescott and Mulvaney[24] were able to successfully match DDA predictions for these types of gold rods to the observed peak positions but only if they assumed that the rods were pure cylinders. However, the assumption of flat cylinders is not in accord with the usual high-resolution images of these rods, which typically show clear evidence for end capping.

It is crucial to decide whether the lack of agreement between experiment and theory is due to numerical errors introduced by the calculation procedure or to some unconsidered physical phenomenon. Consequently, in this paper, we consider whether atomic roughness is a possible cause of some of the observed redshift. Surface plasmon resonances are notoriously sensitive to sharp edges and protuberances, which act as local "hot spots." Faceting of the gold surface in order to form rodlike particles is accompanied by the exposure of high-energy crystal surfaces. Reorganization and reconstruction may produce small-scale roughness, in addition to any intrinsic roughness due to lattice defects and stacking faults. These defects have been directly observed by Chang *et al.*,[2] Wang *et al.*[25] and also by Gai and Harmer in high-resolution TEM studies of electrochemically and chemically prepared gold rods.[26] Such roughness may alter the surface plasmon energy and may be as important as polydispersity or particle geometry in determining the ensemble optical properties. We will demonstrate on the basis of electrostatic calculations that the SPL mode in nonspherical gold particles is very sensitive to atomic level roughness and crystallographic reconstruction. Based on the results, we conclude that both end-cap geometry and surface roughness play a significant role in determining the actual extinction spectrum and hence perceived color of chemically grown gold rods.

II. THEORETICAL APPROACH

In order to improve the computational efficiency of the modeling, in this work, we use a surface integral (SI) approach to calculate the absorption spectra of small metal particles of arbitrary shape. This technique has previously been

employed by Fuchs[27] to calculate depolarization factors of solids but has not found wide application. It is important to note that the SI approach does not include retardation in the form it is used here, whereas the DDA and other methods do. This restricts the application of the SI technique to smaller particle sizes (quasistatic approximation), i.e., to those with a radius a much smaller than the corresponding surface plasmon resonance wave vector ($a \ll \lambda/2\pi n$). However, the advantage of this technique is that it drastically reduces the CPU time for calculation of the absorption spectra so that a very fine sampling of the electromagnetic properties can be achieved. This makes it a more suitable technique for particles with sharper edges. Complete spectra can be calculated on a personal computer in a few minutes using the SI approach. Furthermore, it should be noted that according to Draine and Flatau,[16] gold nanorods may be one of the less favorable systems to which to apply the DDA model.

Another important aspect of the quasistatic approximation is the possibility to directly test the accuracy of the calculations. This can be done because there is an analytical solution for the particular case of spheroids.[28] We find that the SI calculations reproduce the depolarization factors of spheroids with axial ratios as large as 10 with an error less than 0.5%.

Finally, the SI approach is directly related to the spectral representation formalism,[27,29] and it is therefore possible to decouple the geometric problem from the material properties given by the dielectric function of the body. As a result, a single calculation for each geometry allows the determination of the optical response of the particle for any given dielectric function. According to the spectral representation, the effective dielectric susceptibility along the l direction of a single particle in vacuum is given by

$$\langle \chi \rangle_l = \sum_k \frac{C_{k,l}}{\frac{1}{\chi_p} + L_{k,l}}, \tag{1}$$

where $L_{k,l}$ is the generalized depolarization factor, χ_p is the relative electric susceptibility (taken from Ref. 30), and $C_{k,l}$ is its pole weight. In this work, we will discuss exclusively the effect of the main mode ($k=1$) arising from polarization along the primary axis of the particle ($l=3$ or z axis). To calculate the coefficients, we now follow the surface integral method based on the procedure originally outlined by Fuchs. In fact, specific solutions have been published for parallelepipeds[31] and cubes,[32] which are superpositions of several terms similar to those in Eq. (1), with different weights and values of the depolarization factors, but this procedure cannot be applied directly to curved solids.

Within the quasistatic approximation, the electric field at any point **r** of a solid can be written as

$$\vec{E}(\vec{r}) = \vec{E}_0 + \frac{1}{4\pi\varepsilon_0}\int_S \frac{\vec{P}(\vec{r}')\cdot\vec{n}(\vec{r}')(\vec{r}-\vec{r}')}{|\vec{r}-\vec{r}'|^3} dS' \tag{2}$$

where **P** is the polarization vector, **n** the normal vector to the surface, **r** the position vector, and dS' a surface differential element of the solid. Equation (2) transforms into

$$\frac{\vec{p}(\vec{r})}{\varepsilon_0\chi(\vec{r})} = \vec{E}_0\cdot\vec{n}(\vec{r}) - \frac{\vec{p}(\vec{r})}{2\varepsilon_0} + \frac{1}{4\pi\varepsilon_0}\int_S \frac{\vec{n}(\vec{r})\cdot(\vec{r}-\vec{r}')}{|\vec{r}-\vec{r}'|^3}\vec{p}(\vec{r}')dS', \tag{3}$$

where we define $\vec{p}(\vec{r}) = \vec{P}(\vec{r})\cdot\vec{n}(\vec{r})$. In the case of a cube, Fuchs employed the cubic O_h point group symmetry to reduce the number of matrix elements. In the case of a capped cylinder, there is both axial symmetry and a perpendicular mirror plane ($D_{\infty h}$ point group). This symmetry allows us to analytically integrate Eq. (3) over the rotation angle. After the integration along the revolution angle, Eq. (3) can be rewritten as

$$\left(\frac{4\pi}{\chi(z)} + 2\pi\right)p(z) = 4\pi\varepsilon_0\vec{E}_{0,z} + \frac{1}{4\pi\varepsilon_0}\int_{-L}^{L} \frac{R_l\{\Phi_0(\alpha)[n_x R + n_z(z-z')] - \Phi_1(\alpha)n_x R'\}}{n_x\sqrt{[R^2+R'^2+(z-z')^2]^3}}\vec{p}(z')dz', \tag{4}$$

where z and R are the dimensions parallel and perpendicular to the revolution axis, respectively, and

$$\alpha = \frac{2RR'}{R^2+R'^2+(z-z')^2}, \tag{5}$$

$$\Phi_0(\alpha) = \int_0^{2\pi} \frac{1}{\sqrt{(1-\alpha\cos\varphi)^3}}d\varphi = \frac{4E\left(\frac{2\alpha}{\alpha-1}\right)}{\sqrt{1-\alpha}(1+\alpha)}, \tag{6}$$

$$\Phi_1(\alpha) = \int_0^{2\pi} \frac{\cos\varphi}{\sqrt{(1-\alpha\cos\varphi)^3}}d\varphi = \frac{4E\left(\frac{2\alpha}{\alpha-1}\right)}{(1+\alpha)\sqrt{1-\alpha}} - \frac{4K\left(\frac{2\alpha}{\alpha-1}\right)}{\alpha\sqrt{1-\alpha}}. \tag{7}$$

Here, K and E are the complete elliptic integrals of the first and second kind, respectively.[33]

If one takes into account the fact that Eq. (2) is the result of the application of Gauss' theorem to the evaluation of the electric field generated by a dipolar three-dimensional distribution (which is the physical foundation of the nonretarded DDA model), it can be recognized that the transformations from Eq. (2) to Eq. (4) result in a reduction in the dimensionality of the surface integral from three dimensions (corresponding to the DDA model) to only one dimension, with a subsequent increased speed of the calculation.

In order to solve Eq. (4), it can be discretized as follows:

$$\left(\frac{4\pi}{\chi(\vec{r})}+2\pi\right)p_k = 4\pi\varepsilon_0\vec{E}_0\cdot n_{z,k}+\sum_l \tilde{K}_{l,k}p_l w_l, \tag{8}$$

where the nondiagonal term of the kernel of the integral equation is given by

$$K_{\substack{l,k\\k\neq l}} = \frac{R_l\{\Phi_0(\alpha_{k,l})[n_{x,k}R_k+n_{z,k}(z_k-z_l)]-\Phi_1(\alpha_{k,l})n_{x,k}R_l\}}{n_{x,l}\sqrt{[R_k^2+R_l^2+(z_k-z_l)^2]^3}}, \tag{9}$$

and the diagonal term is just the integral value in the interval $\Delta=(z_{k+1}-z_{k-1})/2$ around the value of z_k,

$$K_{k,k} = \int_{z_k-\Delta}^{z_k+\Delta} \frac{R(z')\{\Phi_0[\alpha(z_k,z')][n_{x,k}R_k+n_{z,k}(z_k-z_l)]-\Phi_1[\alpha(z_k,z')]n_{x,k}R(z')\}}{n_{x,l}\sqrt{[R_k^2+R^2(z')+(z_k-z')^2]^3}}dz', \tag{10}$$

which, for small values of Δ, can be approximated as

$$K_{k,k} = \frac{\Delta}{R_k}\left[2.772\,59-\log\left(\frac{\Delta}{n_{x,k}R_k}\right)\right]. \tag{11}$$

Depolarization factors can be obtained from the eigenvalues λ_m of the **K** matrix,

$$\mathbf{K}=\mathbf{P}^{-1}\Lambda\mathbf{P}. \tag{12}$$

The depolarization factors are given by

$$L=\tfrac{1}{2}-\lambda_m, \tag{13}$$

while the corresponding polarization weights of the eigenvalues are given by

$$C_l = 4\frac{\sum_l\left[\text{abs}\left(\sum_k \frac{R_k w_k}{n_{x,k}}P_{kl}\right)\text{abs}\left(\sum_m (P^{-1})_{lm}n_{z,m}\right)\right]}{\sum_l w_l R_l^2}. \tag{14}$$

Note that the coefficients satisfy the following sum rule:

$$\sum_l C_l = 1. \tag{15}$$

We use the SI method to consider the end-cap geometry and surface roughness as follows. Figure 1(a) shows how the end-cap geometry can be varied between that of a flat cylinder and a spherically capped one in terms of the parameter z/a. Figure 1(a) also illustrates a simple mathematical approach to simulating surface roughness. The surface roughness is characterized by the amplitude r and period t of a sinusoidal cross section imposed on the cylinder. Provided that the period is substantially less than the rod length, the periodicity does not play a substantial role, since the effective composition of the rough region does not change with period. Hence, the amplitude, or more precisely, the relative amplitude defined as $\rho=r/a$, is the primary parameter of interest.

III. EXPERIMENTAL PROCEDURE

Gold rods were prepared by a modified version of the seeded growth method proposed by Novo *et al.*[9] and Nikoobakht El-Sayed.[10] This procedure employs silver ions in the synthesis, which converts twinned particles into single

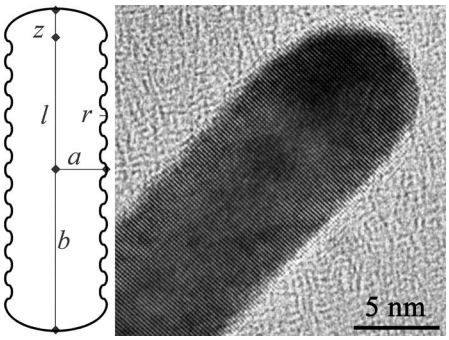

FIG. 1. (a) Outline showing the geometry of the cylinder and the capping geometry. The core cylinder has a length l and radius a. The two end caps have a variable vertical height z, which varies from zero (pure cylinder) to a maximum value of a for a spherically capped cylinder. The length measured in the TEM is $2b=2(l+z)$, and hence the perceived aspect ratio for the capped rod is $AR=b/a$. The surface may consist of small sinusoidal oscillations with an amplitude r and period t. The roughness factor is given by $\rho=r/a$. (b) High-resolution electron micrograph of a single gold rod. Note that the rod surface shows slight roughness. The roughness is estimated to be of order 2–3 lattice atoms high. The mean cap-axial ratio appears to be about $z/a\sim 1.0$. Electron diffraction reveals that the majority of the gold rods are single crystals and grow along the ⟨100⟩ direction.

crystals. The growth direction is ⟨100⟩. In Fig. 1(b), we show a high-resolution electron micrograph, representative of the gold rods used in this study. The aspect ratio in the different samples used varied from about 1.5:1 to 5:1 basically due to a reduction in the rod width, which is 13 nm for less elongated samples and which decreases to 6.5 nm for elongated rods. Each sample exhibits a Gaussian distribution of aspect ratios with a standard deviation of about 10%. As shown previously for this level of polydispersity, the SPL band peak position does not vary appreciably from the position of the mean.[24] At higher resolution, the particles appear to be spherically capped, though some particles exhibit faceting [Fig. 1(b)]. What is also clear from the high-resolution micrograph in Fig. 1(b) is that the sides of the rods are not smooth but show evidence for roughness extending some 2–3 planes in depth. This roughness may be due to surface reconstruction or may be induced by the kinetics of particle growth, but it is intrinsic to the rods and is regularly seen at high resolution on single rods.

IV. RESULTS AND DISCUSSION

As we have used a quasistatic approximation [particle size much smaller than the incident wavelength, or $a \ll \lambda/(2\pi n)$] to estimate the electromagnetic response of these nanorods, it is mandatory to be sure that this approximation holds for the small gold nanorods considered here. Consequently, we have carried out several *T*-matrix calculations for elongated spheroids using the software AMPLD, originally written by Mishchenko[34] and recently modified by Moroz.[35] This program was specifically designed to carry out computations on strongly absorbing materials. Even in the worst case (spheroids with axial ratio of 5 and a 10 nm thickness), only a 3 nm shift is predicted due to retardation and scattering effects. The quasistatic approximation should therefore be applicable to the gold rods. Figure 2 shows the experimental optical spectra of the gold rods and the fits obtained with and without the inclusion of surface roughness. The SI calculations reproduce the peak positions well, though the introduction of surface roughness clearly improves the agreement with theory. It is also evident that the theoretical peak widths are much smaller than the experimentally determined ones. Surface damping of the conduction electrons was included in the dielectric function of the gold rods; however, this clearly does not account for the spectral width observed experimentally. The surface plasmon band width is inhomogeneously broadened by particle polydispersity. Consequently, we do not attempt to reproduce the experimental peak widths. Recent dark field microscope measurements of the surface plasmon (SP) bandwidth of single gold rods have demonstrated that surface scattering and radiation damping corrections successfully account for the SP peak width.[9] In Fig. 3(a), we plot the observed SPL band peak positions (large dots) and the results of SI modeling for smooth rods with different end-cap geometries (lines). The aspect ratios of the gold nanorods were estimated from the statistically determined mean length and width of the rods observed by TEM. It can be seen that for each aspect ratio, there is a systematic redshift as the end-cap geometry is altered from spherical to flat,

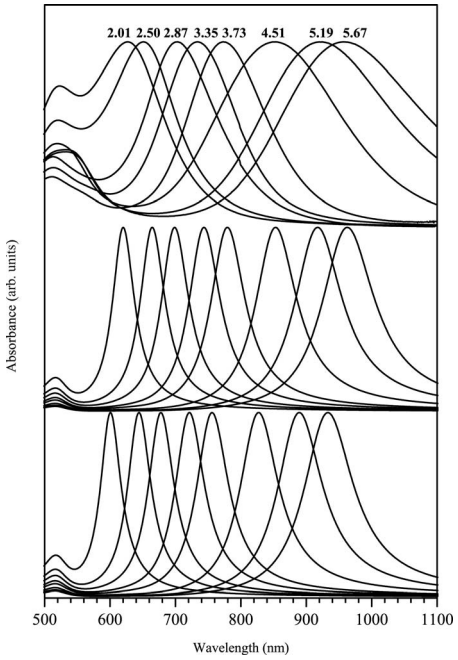

FIG. 2. Experimental optical spectra of Au nanorods with increasing aspect ratios (AR=2.01, 2.50, 2.87, 3.35, 3.73, 4.51, 5.19, and 5.67) (top) compared with theoretical calculations for rough (ρ=0.04) nanorods (middle) and smooth ones (bottom).

corresponding to the case of a pure cylinder. This redshift is practically independent of the aspect ratio and its value is around 50 nm.

However, from TEM micrographs [Fig. 1(b)], it is clear that the most common end cap is the hemispherical one. Hence, it is not possible to justify the experimentally observed redshift, compared to the position predicted for spheroids [thin line in Figs. 3(a) and 3(b)] exclusively from the geometry of the nanorod. In Fig. 3(b), the experimental po-

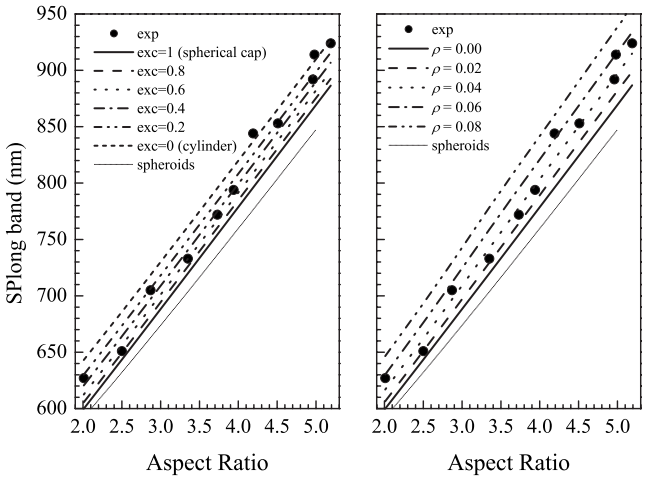

FIG. 3. (a) Comparison of experimental (big dots) SPL peak positions and SI calculations (lines) for different cap geometries (exc=z/a), from hemispherical to planar. (b) Comparison of experimental (big dots) SPL peak positions and SI calculations (lines) for different hemispherical geometry and small values of roughness. Exact SPL peak positions for spheroids appear as short dotted line.

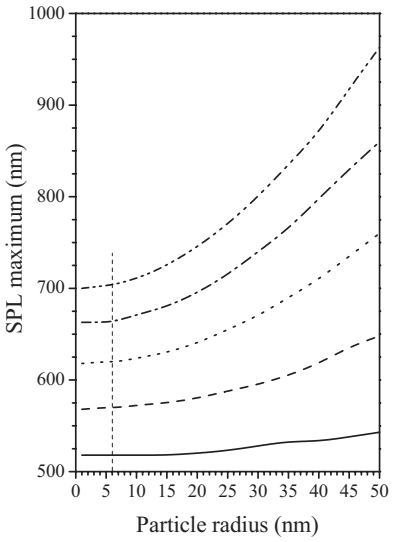

FIG. 4. SPL wavelength of spheroids as a function of the aspect ratio for different cap-axial ratios (continuous line, axial ratio AR =1; dashed, AR=2; dotted, AR=3; dashed-dotted, AR=4; dashed-dotted-dotted AR=5). Vertical dashed line indicates the average nanorod radius.

sitions of nanorods with different aspect ratios are compared to those calculated for nanorods with hemispherical cap-axial ratios ($z/a=1.0$), but with various surface roughness amplitudes given by $\rho=r/a$. In this case, a good fit is obtained for roughness values of about $\rho \sim 0.02-0.06$ depending on the type of sample. We thus find that one may justifiably fit the mode position by varying the apparent end-cap curvature or surface roughness amplitude within realistic limits determined by electron microscopy.

As noted by other authors, the peak position of the SPL band shows a linear dependence on aspect ratio but is substantially redshifted from the predictions of the simple analytical Gans (ellipsoid) model. Link *et al.* initially suggested that the redshift was due to an increase in the local refractive index around the particles due to either ordered water or surfactant molecules.[6,36] However, it is not possible to obtain agreement unless unrealistic values for the layer thickness and the refractive index are used. The second mechanism to induce a redshift is the effect of retardation, especially in the case of large particles. However, according to Fig. 4, it is expected that nanorods with a width smaller than 10 nm should not exhibit a significant redshift. In this work, we have argued that both end-cap geometry and surface roughness may be important. Thus, there are two mechanisms to account for the plasmon mode peak positions. We can flatten the end caps to induce a red shift or we can increase the surface roughness. Based on the electron micrographs of our samples, we believe that the rods may be better modeled as capped cylinders. We may approximately model the data if the end cap is assumed to have a ratio of $z/a=0.2$. This is not inconsistent with the high-resolution electron micrographs, though these generally indicate a rounder geometry close to $z/a \sim 1.0$. The depolarization factors for capped cylinders still lead to an almost linear dependence of the SP peak wavelength on the rod aspect ratio, but the slope of the plots becomes a strong dependant function of the end-cap curvature.

Our calculations clearly indicate that the SPL mode is sensitive to structural details at the atomic scale. This is another phenomenon (not previously detected in larger ellipsoidal particles at infrared wavelengths[37,38]) exclusively related to the nanometer scale of the nanocrystals. This is because the atomic disorder is just 2 orders of magnitude smaller than the width of the nanorods. Interestingly, the introduction of surface roughness into gold spheres does not result in a significant red shift;[25] hence, it is possible that surface roughness is present and important in determining the SPL peak position but that its role is discernible only in nonspherical geometry. These results also indicate that it will not be possible to deduce the geometry of a metal particle purely from its surface plasmon resonance scattering or extinction properties without detailed structural information.

The physical reason for the strong dependence of roughness and end-cap geometry on SPL peak position is related to the influence of the edges and vertices on the electrostatic distribution of charges (Fig. 5). In the case of nanorods, both end-cap geometry and roughness are associated with areas of very large curvature. According to the work of Beagles and Whiteman,[39] which is based on the solution to Poisson's equation for a conical geometry, the polarization around a vertex follows a power law divergence. The first important consequence of this result is that it is necessary to sample the polarization with a large number of points around the irregular parts of the solid bodies in order to accurately calculate the electromagnetic field around the solid. The SI approximation enables an enormous increase in the accuracy of quasistatic calculations without a significant calculation time cost. The second important consequence is that small areas of the rod or particle with large values of surface curvature may strongly modify the polarizability of the whole body. To illustrate this point, we have calculated the depolarization factor of a nanorod with just a single dip in the center of the rod, similar in depth to the considered surface roughness. The result, shown in Fig. 5, is that just a single dip induces a similar redshift in the SPL peak as the previously calculated roughness [Figs. 3(a) and 3(b)]. As a rule of thumb, the most relevant parameter to determine the SPL position of metallic nanorods is the ratio of the maximum length of the rod to the minimum value of the rod thickness. Conversely, engineering surface roughness may provide an alternative method for tuning the peak position.

V. CONCLUSIONS

We have shown that the SPL mode of gold nanorods is extremely sensitive to the atomic scale roughness of the rod surface, despite the spectra being calculated in the nonretarded, long-wavelength (or dipole) limit. Numerous authors have found large discrepancies between the theoretical and experimental SPL peak positions of these types of small gold and silver particles. The introduction of capped cylindrical geometry improves the agreement, but the differences can be equally explained in terms of atomic level surface roughness.

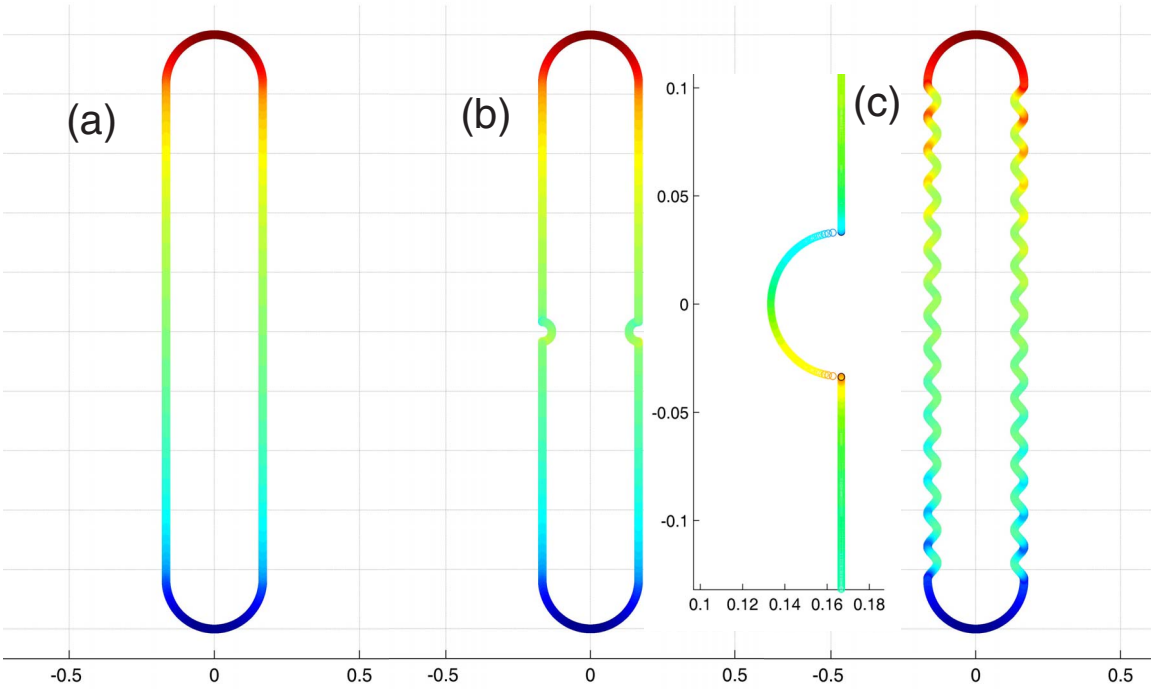

FIG. 5. (Color online) Polarization distribution induced by an external electric field on the surface of (a) elongated rod of AR=6 and hemispherical cap and (b) rod similar to that of (a) but with a defect of radius ρ=0.1. An inset has been included to show the polarization distribution around the dip; (c) rod similar to that of (a) but with roughness ρ=0.1.

In general, surface roughness leads to pronounced redshifts of the SPL mode. We believe that the improved computational efficiency of the surface integral method will prove useful in the calculation of the optical properties of small metal nanostructures. In addition, on the basis of the results shown here, incorporating surface roughness should improve the agreement with experiment and in the design of plasmonic structures. It can also be envisaged that lithographic methods may be used to construct optimized plasmonic structures with tailored roughness and ultrahigh surface electric field enhancement factors.[9]

ACKNOWLEDGMENTS

This work has been supported by the Spanish Ministerio de Educación y Ciencia (Project Nos. MAT2004-02991, PCI2005-A7-0075, and MAT2006-10249C02-01) and the ARC through Grant Nos. DP 0344356, DP0558608 and FF0561486.

[1] Y.-Y. Yu, S. S. Chang, C. L. Lee, and C. R. C. Wang, J. Phys. Chem. B **101**, 6661 (1997).
[2] S.-S. Chang, C. W. Shih, C. D. Chen, W.-C. Lai, and C. R. C. Wang, Langmuir **15**, 701 (1999).
[3] N. R. Jana, L. Gearheart, and C. J. Murphy, J. Phys. Chem. B **105**, 4065 (2001).
[4] N. R. Jana, L. Gearheart, and C. J. Murphy, Chem. Commun. (Cambridge) **2001**, 617.
[5] I. Lisiecki and M. P. Pileni, J. Am. Chem. Soc. **115**, 3887 (1993).
[6] S. Link, M. B. Mohamed, and M. A. El-Sayed, J. Phys. Chem. B **103**, 3073 (1999).
[7] B. M. I. van der Zande, M. R. Böhmer, L. G. J. Fokkink, and C. Schönenberger, J. Phys. Chem. B **101**, 852 (1997).
[8] B. M. I. van der Zande, M. R. Böhmer, L. G. J. Fokkink, and C. Schönenberger, Langmuir **16**, 451 (2000).
[9] C. Novo, D. Gomez, J. Pérez-Juste, Z. Zhang, H. Petrova, M. Reisman, P. Mulvaney, and G. V. Hartland, Phys. Chem. Chem. Phys. **8**, 3540 (2006).
[10] B. Nikoobakht and M. A. El-Sayed, Chem. Mater. **15**, 1957 (2003).
[11] C. J. Johnson *et al.*, J. Mater. Chem. **12**, 1765 (2002).
[12] I. Pastoriza-Santos and L. M. Liz-Marzan, Nano Lett. **2**, 903 (2002).
[13] T. K. Sau and C. J. Murphy, J. Am. Chem. Soc. **126**, 8648 (2004).
[14] K. Arya, Phys. Rev. B **74**, 195438 (2006).
[15] M. Grzelczak, J. Pérez-Juste, F. J. García de Abajo, and L. M. Liz-Marzán, J. Phys. Chem. C **111**, 6183 (2007).
[16] B. T. Draine and P. J. Flatau, J. Opt. Soc. Am. A **11**, 1491 (1994).
[17] N. Felidj, J. Aubard, and G. Levi, J. Chem. Phys. **111**, 1195 (1999).
[18] M. M. Miller and A. A. Lazarides, J. Phys. Chem. B **109**, 21556 (2005).
[19] K.-S. Lee and M. A. El-Sayed, J. Phys. Chem. B **109**, 20331

(2005).
[20] A. Brioude, X. C. Jiang, and M. P. Pileni, J. Phys. Chem. B **109**, 13138 (2005).
[21] P. K. Jain, S. Eustis, and M. A. El-Sayed, J. Phys. Chem. B **110**, 18243 (2006).
[22] T. Wriedt, Part. Part. Syst. Charact. **15**, 67 (1998).
[23] M. M. Miller and A. A. Lazarides, Abstracts of Papers of The American Chemical Society, 231st ACS National Meeting, Atlanta, GA, 2006 (unpublished).
[24] S. W. Prescott and P. Mulvaney, J. Appl. Phys. **99**, 123504 (2006).
[25] K. F. H. Wang, R. A. Drezek, and N. J. Halas, Appl. Phys. B: Lasers Opt. **84**, 191 (2006).
[26] P. L. Gai and M. A. Harmer, Nano Lett. **2**, 771 (2002).
[27] R. Fuchs, Phys. Rev. B **11**, 1732 (1975).
[28] J. A. Osborn, Phys. Rev. **67**, 351 (1945).
[29] D. J. Bergman, Phys. Rep., Phys. Lett. **43**, 377 (1978).
[30] T. Ung, L. M. Liz-Marzan, and P. Mulvaney, Colloids Surf., A **202**, 119 (2002).
[31] D. Langbein, J. Phys. A **9**, 627 (1976).
[32] R. Fuchs, Phys. Lett. **48**, 353 (1974).
[33] K. B. O. J. Spanier, *An Atlas of Functions* (Hemisphere, Washington, 1987).
[34] M. I. Mishchenko, J. Opt. Soc. Am. A **8**, 871 (1991).
[35] A. Moroz, Appl. Opt. **44**, 3604 (2005).
[36] B. Yan, Y. Yang, and Y. Wang, J. Phys. Chem. B **107**, 9159 (2003).
[37] S. Hayashi, N. Nakamori, and H. Kanamori, J. Phys. Soc. Jpn. **46**, 176 (1979).
[38] J. E. Iglesias, M. Ocana, and C. J. Serna, Appl. Spectrosc. **44**, 418 (1990).
[39] A. E. Beagles and J. R. Whiteman, Math. Methods Appl. Sci. **11**, 215 (1989).